Electronic Supplementary Material (ESI) for Catalysis Science & Technology.

SUPPLEMENTARY INFORMATION

Theta-1 zeolite catalyst for increasing the yield of propene when cracking olefins and its potential integration with an olefin metathesis unit

*Vincent Blay[1], Pablo J. Miguel[1] and Avelino Corma[2]**

[1]Departamento de Ingeniería Química, Universitat de València, Av. de la Universitat, s/n, 46100 Burjassot, Spain

[2]Instituto de Tecnología Química, Universitat Politècnica de València-Consejo Superior de Investigaciones Científicas, Avenida de los Naranjos s/n, 46022 Valencia, Spain

*Corresponding author acorma@itq.upv.es

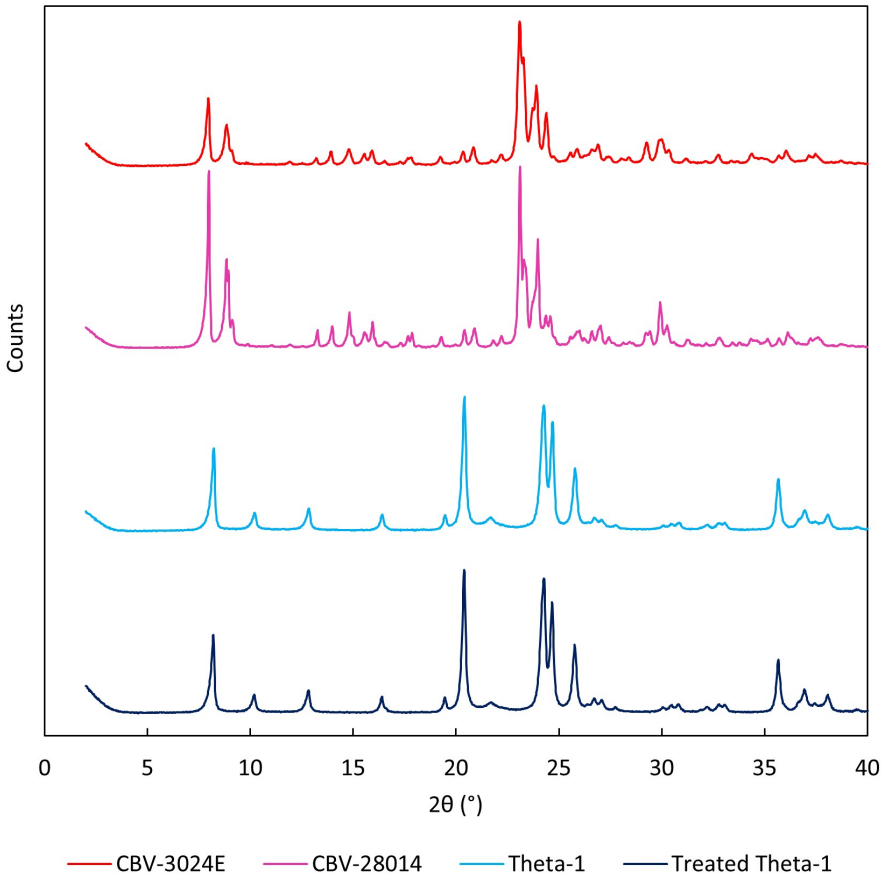

Figure S1. Powder X-ray diffractograms of the zeolite samples investigated.

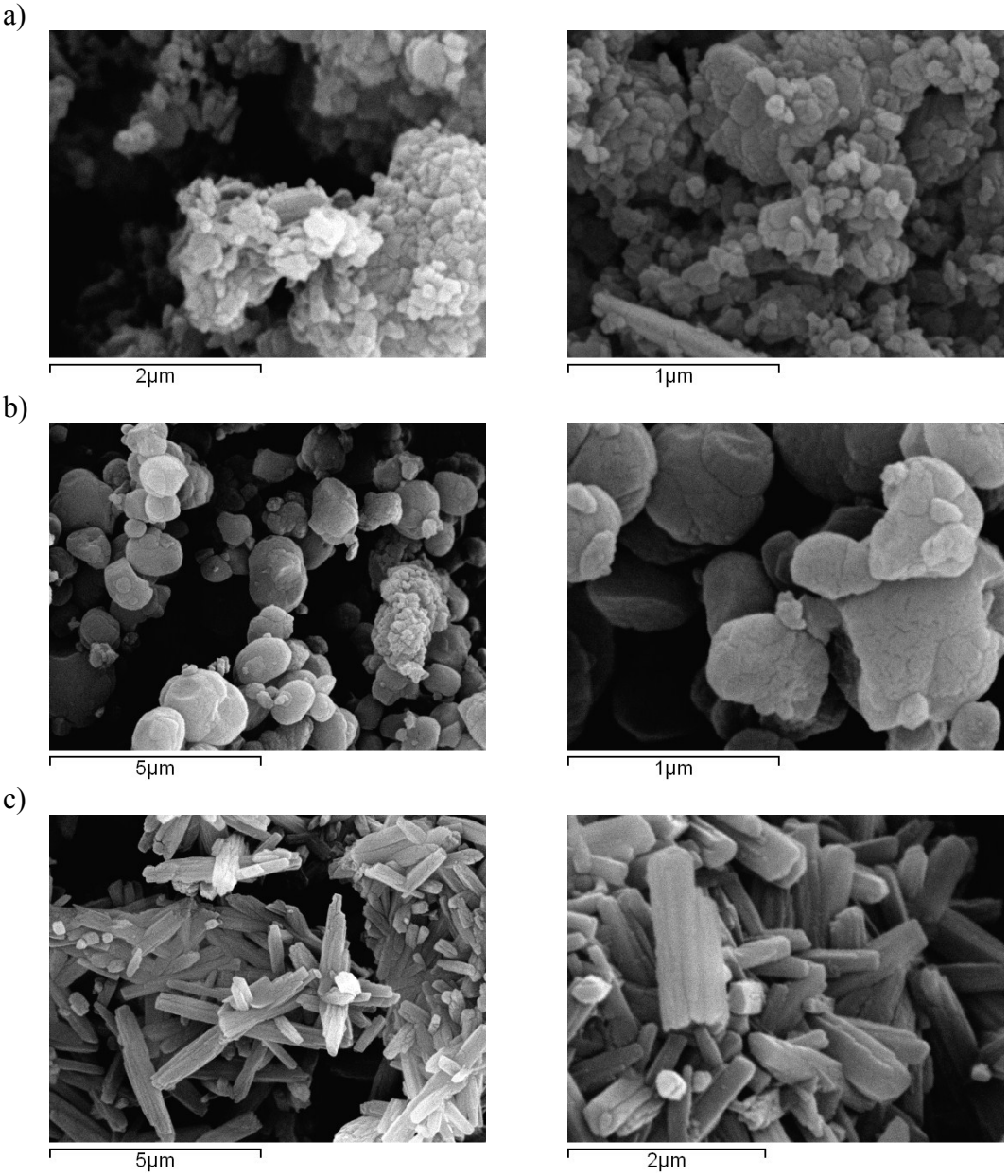

Figure S2. Scanning electron microscopy images of the zeolite samples investigated: a) CBV-3024E, b) CBV-28014, c) Theta-1.

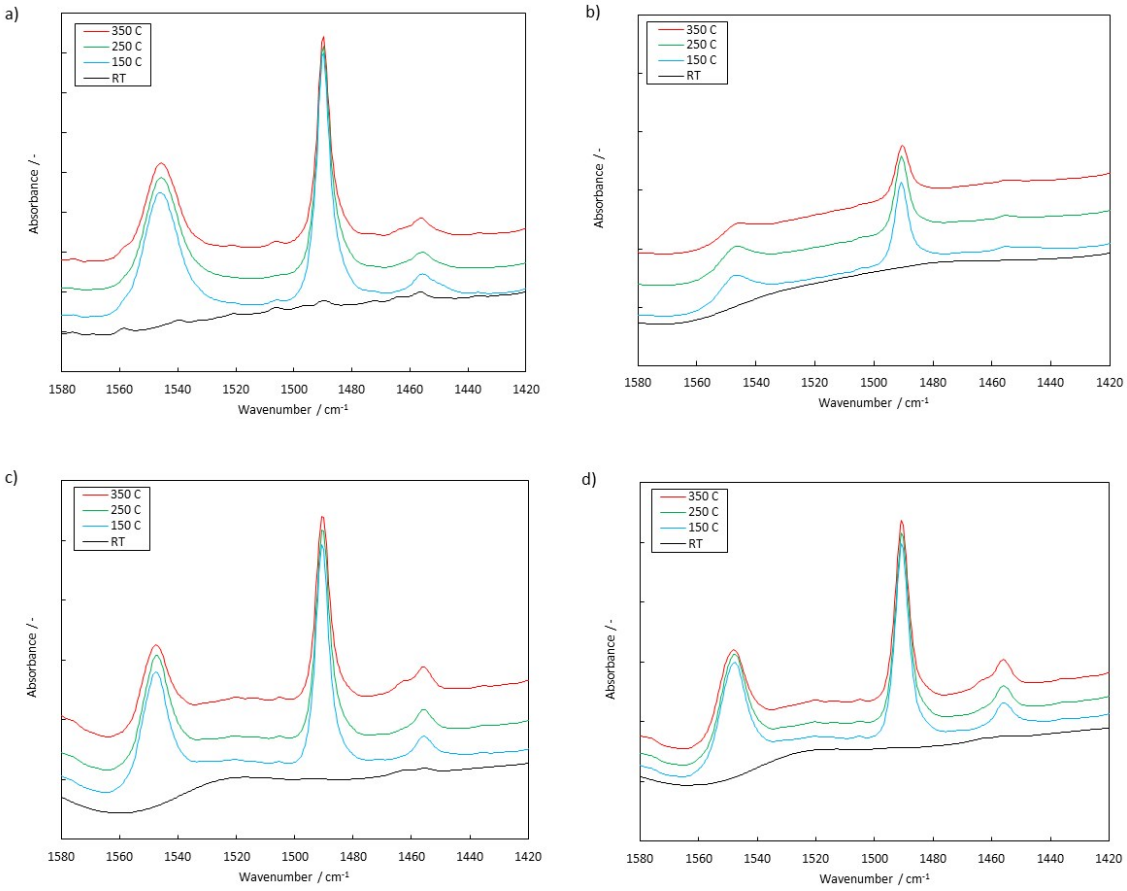

Figure S3. Pyridine-FTIR spectra of the zeolite samples: a) CBV-3024E, b) CBV-28014, c) Theta-1, d) treated Theta-1. Distance between y-axis ticks is 0,2 absorbance units.

Table S1. Textural properties of selected zeolite samples.

Zeolite sample	BET area / $m^2\ g^{-1}$	V_{micro} / $cm^3\ g^{-1}$	V_{meso} / $cm^3\ g^{-1}$	Crystal size[a] / µm
Theta-1	189	0.082	0.029	1-2
CBV-3024E	372	0.162	0.068	0.3-0.6
CBV-28014	369	0.161	0.076	1-2
Treated Theta-1	226	0.088	0.096	0.5-1

[a]Estimated from SEM images.

Table S2. Acidity determination of studied materials by pyridine-FTIRS. Bxxx and Lxxx represent the amount of pyridine molecules that remain adsorbed on Brønsted and Lewis acid sites at T = xxx °C, respectively.

Zeolite sample	B150	B250	B350	L150	L250	L350	Total acid content / µmol g^{-1}	Si/Al[a]	Total Al content[a] / µmol g^{-1}
Theta-1	200 92 %	178 82 %	129 60 %	16 8 %	15 7 %	15 7 %	216 100 %	44	352
CBV-3024E	377 93 %	343 85 %	285 70 %	29 7 %	30 7 %	29 9 %	406 100 %	15	1122
CBV-28014	58 96 %	53 88 %	31 51 %	4 6 %	2 3 %	2 3 %	62 100 %	123	138
Treated Theta-1	179 90 %	162 82 %	132 67 %	19 10 %	18 9 %	18 9 %	198 100 %	46	337

[a]Measured by ICP-AES.

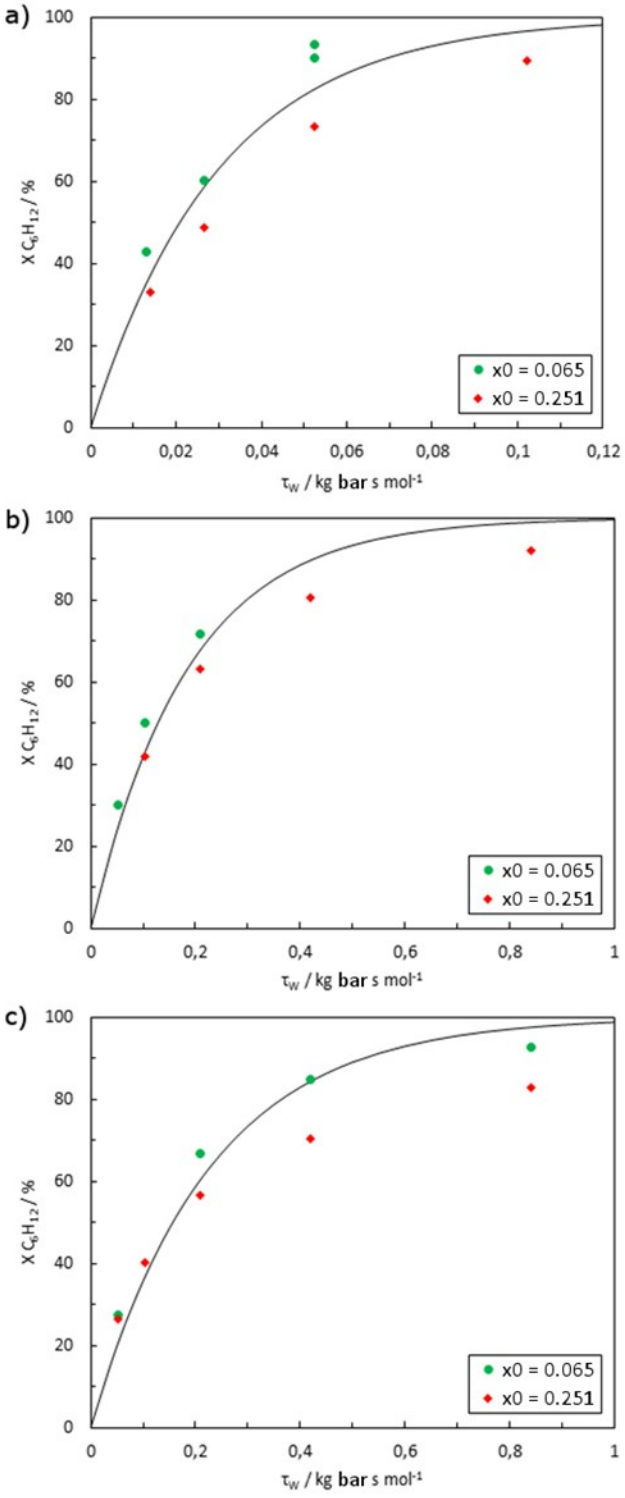

Figure S4. Conversion of 1-hexene over a) CBV-3024E, b) CBV-28014, and c) Theta-1 as a function of the modified contact time, τ_W. Solid lines correspond to the unweighted regression to first order kinetics as reported in Table 2.

External and internal mass transfer

As for the apparent orders slightly below 1 observed in the article, one might think that the kinetics could follow a more complex law, like Langmuir-Hinshelwood-Hougen-Watson models, in which there is a competition for sites. However, we demonstrated that hydrocarbon adsorption, and in particular, acid site coverage is very low in the cracking of alkanes at high temperatures (1). Alternatively, the fast cracking rates of 1-hexene on zeolites may decrease the catalysts effectiveness factors, more at higher partial pressures, leading to apparent deviations from a reaction order of unity upon data fitting.

To assess external mass-transfer limitations in the catalytic cracking results, we estimated the external mass transfer coefficient, k_c, from Frössling's correlation (2):

$$k_c = \frac{Sh\, D_{AB}}{d_p} \qquad (1)$$

$$Sh = 2 + 0.6\, Sc^{0.6}\, Re^{0.66} \qquad (2)$$

For the sake of being conservative, the highest possible gas resistance was considered (Re = 0, Sh = 2) and a large pellet diameter of 0.5 mm. The diffusivity of 1-hexene in helium was estimated from the Fuller, Schettler and Giddings' correlation (3):

$$D_{AB} = \frac{0.01\, T^{1.75} \left(\frac{1}{M_A} + \frac{1}{M_B}\right)}{P\left(\sum v_A^{1/3} + \sum v_B^{1/3}\right)^2} \qquad (3)$$

From a balance in the gas layer around the particle the difference in hexene concentration across the boundary layer can be evaluated:

$$\Delta c_{film} = c_A - c_{AS} = \frac{r}{S_p\, k_c} \qquad (4)$$

where r is the hexene reaction rate and c_{AS} is the concentration of hexene at the pellet surface. We estimated the maximum value for r from the results at the shortest $WHSV^{-1}$.

$$r = \frac{F_{A0} X}{W} \qquad (5)$$

Pellets were considered spheres, which has the lowes possible surface-to-volume ratio. To check for internal mass-transfer limitations, the Weisz-Prater criterion was considered:

$$C_{WP} = \frac{r\, \rho_p\, R_p^2}{D_{TA}^e c_{AS}} \qquad (6)$$

In the absence of internal diffusion limitations, $C_{WP} \ll 1$. D_{TA}^e is the effective diffusivity of hexene inside the pellet. Pellets of pressed zeolites often show pore diameters in the range of hundreds of nanometers (4). In those conditions Knudsen diffusion, in addition to molecular diffusion, becomes relevant. Assuming a pore radius of 300 nm, Knudsen diffusivity was estimated according to the ideal gas theory:

$$D_{KA} = 3.068\, R_{pore} \left(\frac{T}{M_A}\right)^{1/2} \qquad (7)$$

and the transition diffusivity in the pores was approximated by the Bosanquet equation (2):

$$\frac{1}{D_{TA}} = \frac{1}{D_{AB}} + \frac{1}{D_{KA}} \qquad (8)$$

the transition diffusivity has to be further corrected with the porosity, $\bar{\varepsilon}$, and tortuosity, τ, of the pellet, for which rough values of 0.5 and 4 were used, respectively:

$$D_{TA}^{e} = \frac{\bar{\varepsilon}}{\tau} D_{TA} \qquad (9)$$

In Table S3, calculations on mass transfer phenomena are presented. It can be seen that, indeed, external diffusion may limit the observed rates to a certain extent, especially for the most active CBV-3024E zeolite catalyst. In that case, the reactant concentration at the surface of the catalyst could be about 20-30 % lower than it would be in a process only controlled by the reaction kinetics. In the less active CBV-28014 and Theta-1, that decrement is estimated to be smaller, around 5 %. Moreover, internal mass-transfer limitations could arise given the fast reaction rates even in the small pellets used at the laboratory scale. Table S3 also presents the results of applying the Weisz-Prater criterion for internal mass transfer. It can be seen that internal mass transfer may limit the cracking rates of the materials studied, especially in the case of CBV-3024E. Indeed, apparent TOF values (roughly estimated by normalizing the initial reaction rate by the Al content) are about 30 % lower on CBV-3024E than on CBV-28014. The even lower TOF values for Theta-1 could be related to its inherently lower acid strength and to incracrystal diffusion, as discussed in the article.

Table S3. Assessment of external and internal mass transfer limitations.

Catalyst	x_0	X / %	r / mol s^{-1} kg^{-1}	c_0 / mol m^{-3}	c_S / mol m^{-3} (a)	Δc_{film} / mol m^{-3} (a)	$\Delta c_{film}/c_0$ (a)	C_{WP} (b)	TOF / s^{-1}
CBV-3024E	0.251	32.9	7.12	3.95	3.73	0.86	22 %	13.7	7.0
CBV-28014	0.251	45.1	1.43	3.95	3.91	0.15	4 %	2.5	10.0
Theta-1	0.251	26.4	1.46	3.95	3.90	0.19	5 %	2.9	4.2
Treated Theta-1	0.251	38.0	2.28	3.95	3.88	0.26	7 %	4.2	6.8
CBV-3024E	0.065	42.7	2.77	1.02	0.72	0.31	31 %	19.1	2.7
CBV-28014	0.065	30.2	0.44	1.02	0.97	0.05	5 %	3.4	3.1
Theta-1	0.065	27.6	0.40	1.02	0.97	0.05	5 %	3.1	1.1

Treated Theta-1	0.065	40.9	0.65	1.02	0.95	0.07	7 %	4.5	1.9

[(a)] $D_{AB} = 1.42 \cdot 10^{-4}$ m^2 s^{-1}
[(b)] $D_{TA}^{e} = 6.80 \cdot 10^{-6}$ m^2 s^{-1}

Thermodynamic limitations

We have seen (*e.g.* Fig. S4) that at long contact times conversion levels tend to level off at values around 85 and 90 % at high and low feed partial pressure, respectively. This also contributes to deviations in the model fitted. Moreover, these cannot be accounted for diffusional limitations, since reaction rates at high conversion values are lower and efficiency factors for external or internal transport would, in the event, be higher than those at lower conversion levels.

This observation is suggestive of thermodynamic limitations. Consequently, we analyzed the thermodynamics of the system. Chemical equilibrium calculations among cracking products were computed by direct minimization of the Gibbs free energy function of the ensemble of components using the *RGibbs* reactor module in Aspen Plus® V.8.0. The fugacity coefficients were derived from the Peng-Robinson equation of state, which evaluated very close to unity in accordance to the ideal behavior of the gas mixture under the conditions studied.

If we consider all the alkenes in the range C_2-C_7, all the alkanes in this range, methane and the BTX, then the conversion of 1-hexene in equilibrium at 500 °C and at the partial pressures used would be virtually 100 % (results not shown). However, these set of compounds is not representative of the real system, since the formation of methane, alkanes and aromatics is seriously hindered over the medium pore zeolites studied. Accordingly, we reduced the number of components considering that monomolecular cracking of hexene is the prevalent mechanism under the conditions studied. This subset thus consists of ethene, propene, and the different

butene and hexene isomers. Ethyl- and dimethylbutenes were excluded in agreement with our experimental observations. The results are presented in Fig. S5 a) and b). We can see that, very interestingly, thermodynamic restrictions can appear indeed if only the fastest reactions in hexene conversion are considered. These would be lowered at lower partial pressure, in agreement with Le Chatelier-Braun's principle. Since cracking of hexene to propene is faster than the asymmetric cracking to butene and ethene it could be most affected by thermodynamics. In this vein, we further reduced the subset of olefins used to compute the equilibrium only to hexene and propene (Fig. S6 c). We observe that yields to propene may be limited in one-pass reactor, and in fact these yields are pretty close to those over Theta-1 at long contact times.

These results are in agreement with those by Zhang *et al*., who studied very recently the equilibrium between olefins in the ranges C_2-C_4, C_2-C_5, C_2-C_6, and C_2-C_7 (5). Incorporation of thermodynamic information in the kinetic model is not straightforward, as it is also affected by the equilibrium of chemisorption on the catalyst surface. One possible approach is the single-event methodology, like von Arentin and Hinrichsen applied (6) using chemisorption data from the computational chemistry experiments by Nguyen *et al*. (7) Nonetheless, the acid site coverage under the cracking conditions applied is low, as can be estimated from (7) and as we demonstrated experimentally in (1) for the case of alkanes.

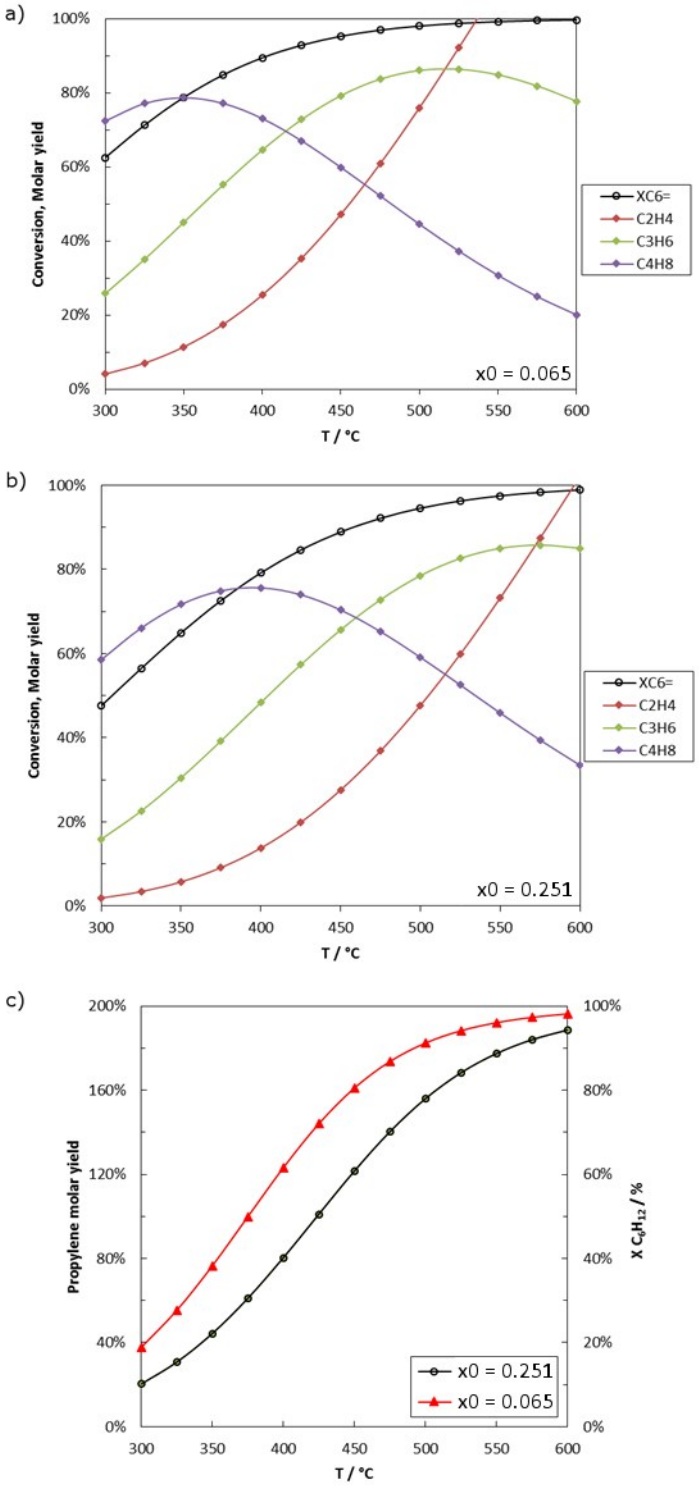

Figure S5. Equilibrium conversion and yields in hexene conversion considering {ethene, propene, butenes, and hexenes} in a) and b), and {propene, hexenes} in c). Ethyl- and dimethylbutenes were excluded from hexenes.

Table S4. Molar yields of 1-hexene catalytic cracking over zeolite materials ($x_0 = 0.065$).

Material	$WHSV^{-1}$ / s	X C_6H_{12} / %	C_2H_4 / %	C_3H_6 / %	*n*-C_4H_8 / %	i-C_4H_8 / %	C_5H_{10} / %	CH_4 / %	C_2H_6 / %	C_3H_8 / %	*n*-C_4H_{10} / %	i-C_4H_{10} / %	C_5H_{12} / %	BTX / %
Theta-1	9.6	27.6	1.7	43.5	0.8	0.2	0.0	0.11	0.07	0.00	0.00	0.00	0.00	0.04
	38.5	66.9	4.1	117.0	1.9	2.3	0.4	0.05	0.07	0.04	0.00	0.00	0.00	0.07
	77.0	85.0	5.7	151.8	3.6	2.0	0.6	0.11	0.09	0.14	0.00	0.00	0.00	0.08
	154.0	92.7	7.2	171.3	3.7	2.4	0.0	0.14	0.14	0.27	0.00	0.00	0.00	0.00
CBV-3024E	2.4	42.7	8.9	56.7	8.0	3.4	1.9	0.00	0.00	0.23	0.00	0.06	0.00	0.08
	4.9	60.3	15.1	78.1	11.2	5.6	2.5	0.17	0.11	0.53	0.00	0.12	0.00	0.13
	9.6	90.2	24.8	114.7	17.1	9.9	2.6	0.21	0.15	1.29	0.13	0.32	0.00	0.20
CBV-28014	9.6	30.2	3.5	40.5	3.1	0.9	0.5	0.05	0.00	0.00	0.00	0.00	0.00	0.04
	19.3	50.2	6.0	66.9	5.0	1.8	1.0	0.00	0.00	0.00	0.00	0.00	0.00	0.07
	38.5	71.8	11.3	107.5	7.5	3.1	2.1	0.00	0.00	0.00	0.00	0.00	0.00	0.07
Treated Theta-1	14.0	40.1	1.9	63.0	0.0	0.6	0.0	0.05	0.05	0.00	0.00	0.00	0.00	0.03
	28.1	58.2	3.2	104.4	0.0	0.5	0.1	0.06	0.07	0.02	0.00	0.00	0.00	0.05
	56.1	80.9	5.3	145.4	3.5	1.7	0.4	0.06	0.09	0.10	0.02	0.00	0.00	0.08

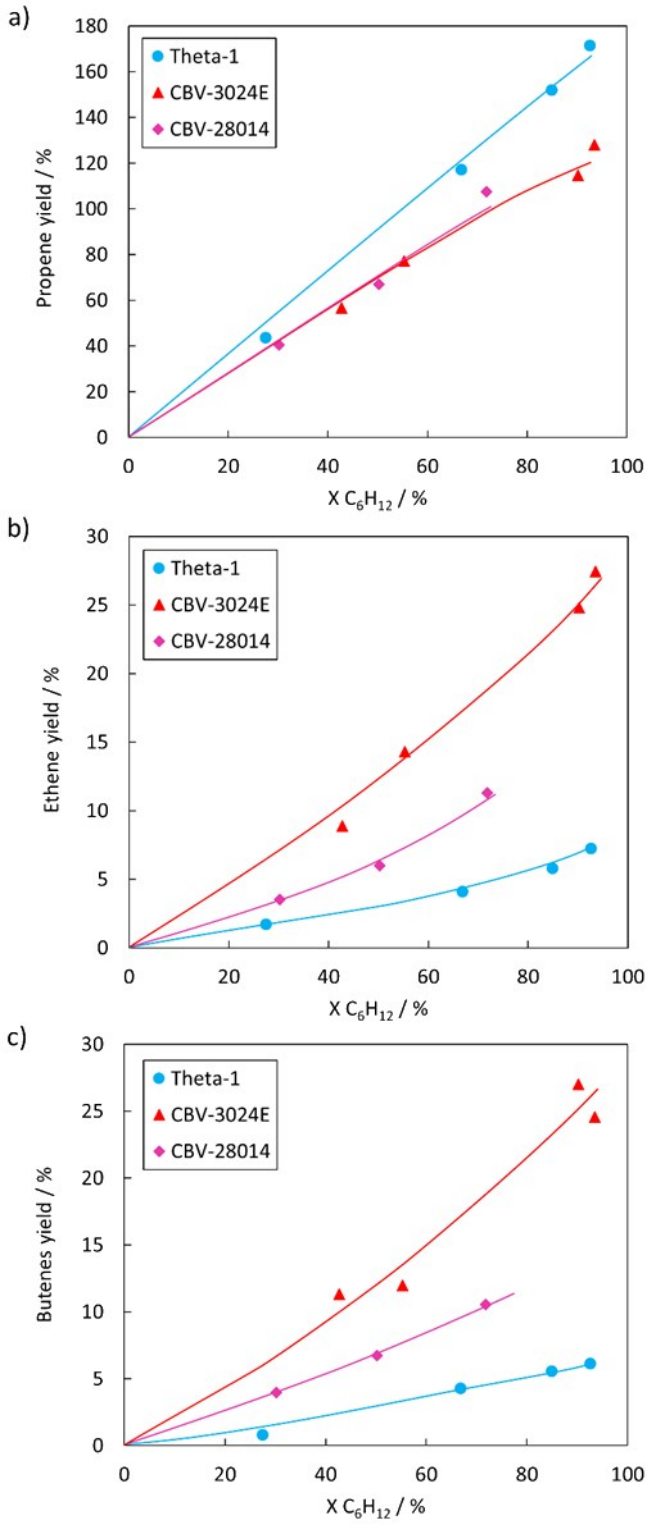

Figure S6. Molar yields to main products *vs*. conversion of 1-hexene cracking at low feed partial pressure (x_0 = 0.065).

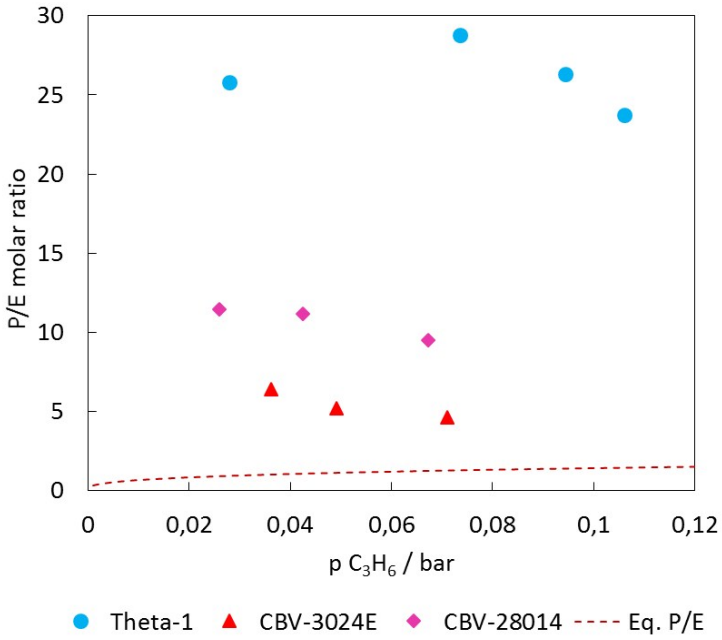

Figure S7. Propene-to-ethene molar ratio (P/E) upon 1-hexene cracking (x_0 = 0.065) and corresponding equilibrium P/E.

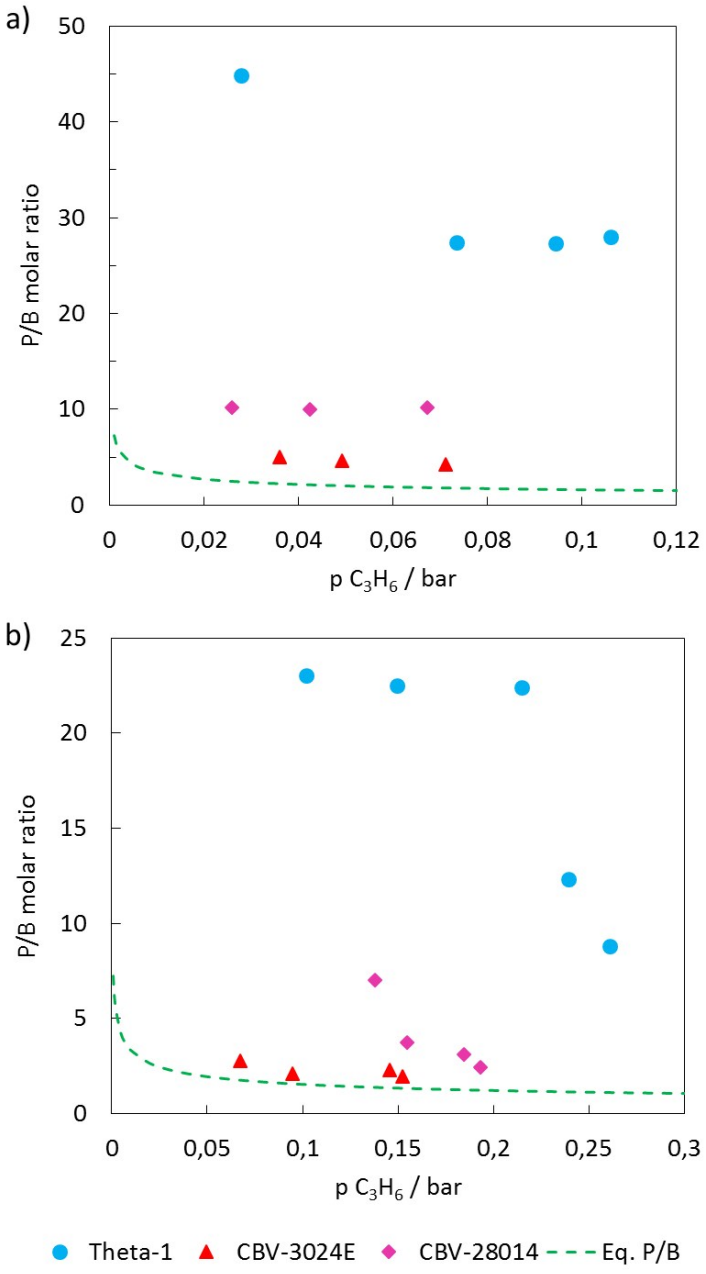

Figure S8. Propene to butenes molar ratio (P/B) upon 1-hexene cracking (a) $x_0 = 0.065$, b) $x_0 = 0.251$) and corresponding equilibrium P/B.

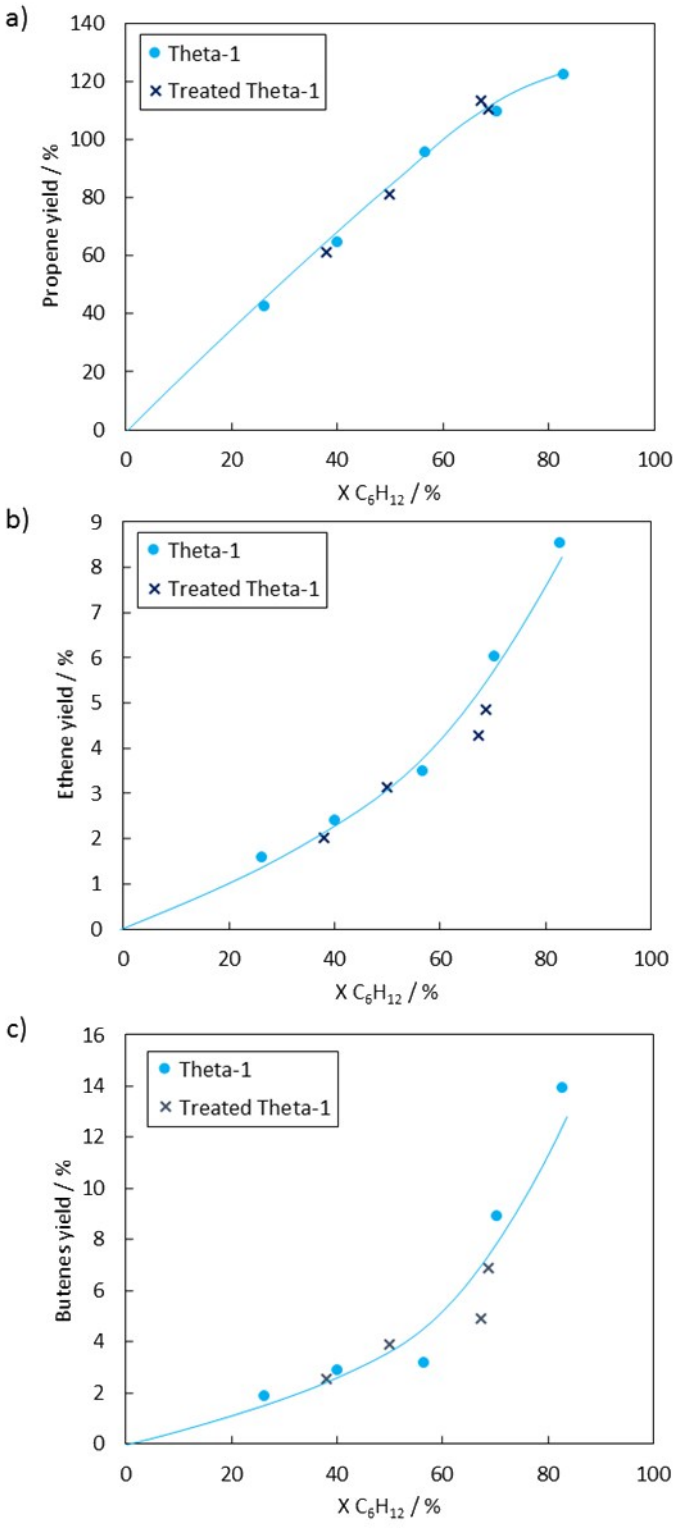

Figure S9. Molar yields to main products *vs*. conversion of 1-hexene cracking at intermediate feed partial pressure (x_0 = 0.251).

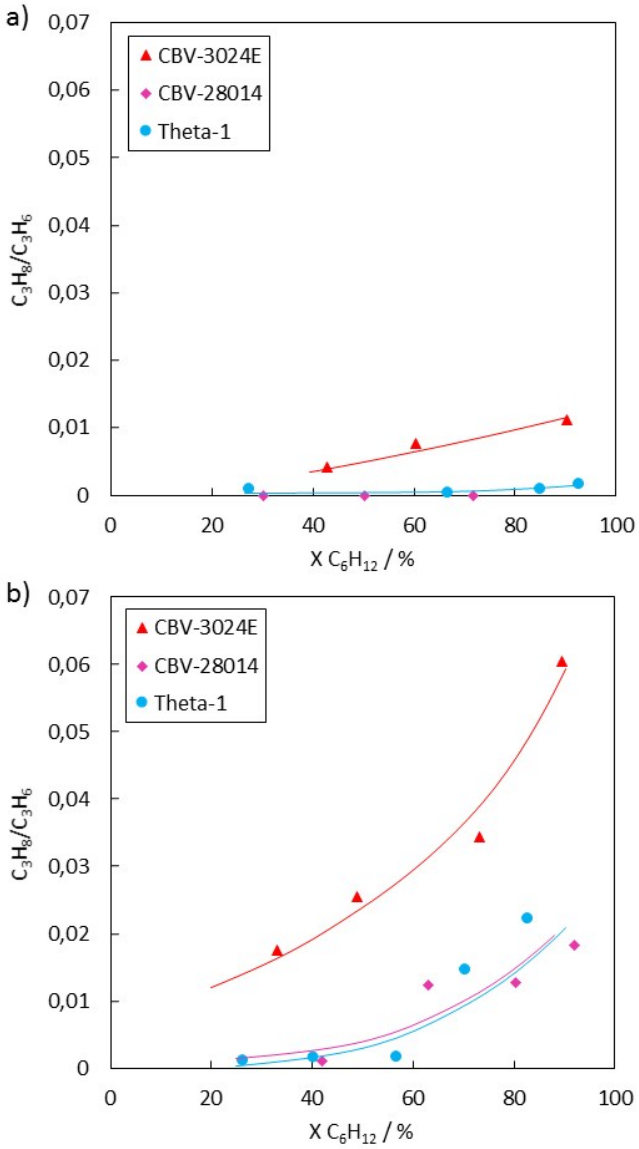

Figure S10. Propane to propene molar ratio in the cracking products: a) $x_0 = 0.065$, b) $x_0 = 0.251$.

References

1. A. Corma, J. Mengual, P. J. Miguel, *J. Catal.,* 2015*,* **330**, 520-532.

2. M. E. Davis, R. J. Davis, *Fundamentals of chemical reaction engineering*; McGraw-Hill: 2003.

3. J. R. Welty, C. E. Wicks, R. E. Wilson, G. Rorrer, *Fundamentals of Momentum, Heat and Mass Transfer, 5th ed.*; John Wiley & Sons: 2006.

4. T. Masuda, *Catal. Surv. Asia,* 2003*,* **7,** 133-144.

5. R. Zhang, Z. Wang, H. Liu, Z. Liu, G. Liu, X. Meng, *Appl. Cat., A*, 2016, **522**, 165-171.

6. T. von Aretin, O. Hinrichsen, *Ind. Eng. Chem. Res.,* 2014, **53**, 19460-19470.

7. C. M. Nguyen, B. A. De Moor, M. Reyniers, G. B. Marin, *J. Phys. Chem. C,* 2011, **115**, 23831-23847.